Received: 22 November 2023 | Revised: 20 March 2024 | Accepted: 22 April 2024

DOI: 10.1002/esp.5877

RESEARCH ARTICLE

ESPL WILEY

How quickly does wood fragment in rivers? Methodological challenges, preliminary findings, and perspectives

Borbála Hortobágyi[1] | David Milan[2] | Fanny Bourgeau[1] | Hervé Piégay[1]

[1]UMR5600 Environnement Ville Société, ENS de Lyon, CNRS, Lyon, France

[2]School of Environmental Sciences, University of Hull, UK

Correspondence
Borbála Hortobágyi, UMR5600 Environnement Ville Société, ENS de Lyon, CNRS, Lyon, France.
Email: borbala.hortobagyi@ens-lyon.fr

Funding information
French Biodiversity Agency; Véodis-3D; French National Research Agency; H_2O'Lyon; Environment Ville Société; Fondation Réseau Français des Instituts d'Études Avancées; Grande Lyon la Métropole; Office Français de la Biodiversité; University of Hull

Abstract

Large wood plays a significant role in fluvial ecosystems, influencing river geomorphology and ecology. However, it poses both benefits to river systems and risks, making it essential to understand its dynamics for effective management. A better understanding the wood breakdown process is required to evaluate the flood risk of wood in rivers. This paper aims to evaluate early-stage fragmentation of wood in rivers after being recruited through bank erosion, taking into account its mobility and residence time. Two methods for characterising and monitoring wood fragmentation are suggested and compared: 1) photo-interpretation based on ground and drone photo and 2) terrestrial LiDAR. We used Quantitative Structure Modelling (QSM) of point clouds to accurately simulate the full branching structure of trees. Close relationships exist between photo-interpreted and LiDAR-derived complexity metrics, but a scaled parameter (i.e., diameter) is needed to correlate branching complexity with volume. The debranching process occurs quickly, with a median reduction in branching complexity of over 80% within the initial 2 years. Further research with a larger sample size is necessary to investigate the impact of context – including transportation, submersion, accumulation, and isolation of wood pieces – on the fragmentation process. Field observations indicate that immobile wood pieces can experience a rapid reduction in their branching complexity, similar to the ones that are transported. Partial fine branching structure can be maintained on transported pieces. Both photo-interpretation and terrestrial LiDAR offer complimentary approaches to monitoring wood fragmentation. Photo-interpretation is easily implementable and may be used as a proxy for mechanical fragmentation, while terrestrial LiDAR may be used to monitor 3D wood fragmentation, volume and length evolution, following QSM modelling.

KEYWORDS
branching complexity, photo-interpretation, residence time, terrestrial LiDAR, wood fragmentation

1 | INTRODUCTION

Large wood in rivers is recognised as a key element of the functional interactions that exist in the fluvial system (Gurnell et al., 2002; Harmon et al., 1986), and understanding the wood regime is of importance for river management (Wohl et al., 2019). Wood is a driver of fluvial processes (Montgomery et al., 2003; Piégay & Gurnell, 1997; Sear et al., 2010) and a critical aspect of river ecology (Abbe & Montgomery, 1996; Benke & Wallace, 2003; Senter & Pasternack, 2011). However, because of the potential risks it poses (Conley & Kramer, 2020; De Cicco et al., 2018; Schalko, 2017), wood has been extensively removed from rivers. Today, wood is being

reintroduced because of its growing appreciation for its positive impact (Anlanger et al., 2022; Grabowski et al., 2019; Gurnell, England, & Burgess-Gamble, 2019; Piégay & Landon, 1997). However, achieving balance between benefits and risks requires a better understanding of wood dynamics in rivers.

Subsequent to the recruitment of wood into rivers (e.g., resulting from lateral bank erosion), a series of physical, hydraulic, chemical, and biological processes occur, leading to the breakdown of wood into smaller fragments, particulate, or even dissolved matter during transport and accumulation. This includes, for example, the weakening of wood because of aging, and the acceleration of wood decay caused by weather conditions, periodic wetting and drying (Harmon et al., 1986; Wohl, 2013). Subsequently, logs deposited on alluvial bars during floods may be impacted. Smaller and more mobile fragments provide a nutrient source and represent a significant amount of organic matter (Beckman & Wohl, 2014). This component of the organic carbon cycle has been widely disregarded (Wohl et al., 2017). Wood characteristics, especially size and geometric complexity, influence mobility, retention, storage, or potential flow blockages (Cadol & Wohl, 2010; Gurnell et al., 2002). According to Manners, Doyle, & Small (2007), the majority (~70%) of jam-forming wood is large, typically exceeding one meter. Logjam dynamics are influenced not only by key member size (Abbe & Montgomery, 1996) but also by wood decomposition rate (Sear et al., 2010).

Wood decay, decomposition or breakdown, related to biochemical processes and predominantly caused by dissolved export, has been extensively researched. Numerous factors, such as wood species, geographical location, physicochemical conditions, biology, and geomorphology, have been identified as controlling factors (Abril et al., 2015; Braccia & Batzer, 2008; Collier, 2014; Díez et al., 2002). A significant portion of the literature focuses on the effect of the time spent in the fluvial system in controlling the decay (Aristi et al., 2012; Cadol & Wohl, 2010), but less attention has been paid to the physical mechanisms of fragmentation, concentrating mainly on general tendencies, for instance, reducing the length of logs (Comiti et al., 2006; Iroumé, Ruiz-Villanueva, & Picco, 2017). Fragmentation involves the size reduction of wood into smaller fragments, contributing to debranching. Merten et al. (2013) showed that wood breakage has a greater short-term effect on wood mass reduction than biochemical decay. The study of tree architecture serves multiple purposes, including estimating the ecological function of branches (Newbrey et al., 2005), and improving models of floodplain inundation (Antonarakis et al., 2009). However, the complexity of tree structures is rarely considered in studies of wood dynamics (Merten et al., 2013), leaving gaps in our understanding of the rate of geometric simplification of newly recruited pieces. Considering that changes in wood shape and volume impact recruitment, transport, and accumulation processes, understanding wood fragmentation can improve predictions of wood dynamics and associated risks (Kramer & Wohl, 2017; Wohl et al., 2023).

Advances in remote sensing techniques over the last 10–20 years now permit high resolution modelling of large wood in rivers. In particular LiDAR and SfM make it possible to resolve large wood accumulations with spatial resolutions in the range 150 point/m^2 to 1 point/mm^2 (Boivin & Buffin-Bélanger, 2010; Grigillo et al., 2015; Tonon et al., 2014). SfM has been shown to have a similar point cloud accuracy to LiDAR (Kaiser et al., 2014; Mancini et al., 2013; Ružić et al., 2014), and has a lower cost. Several advances in modelling wood jams have been made allowing for improved estimations of volume (Sanhueza et al., 2022; Spreitzer et al., 2019, 2020a, 2020b) and porosity (Spreitzer et al., 2020b). Tonon et al. (2014) used terrestrial LiDAR to scan jams but also large wood elements, and compared measurements taken manually in the field with those extracted from the point cloud, which had not been modelled, only manually interrogated. Comparison between the two methods provided satisfactory results in the detection of the main wood characteristics needed for volume assessment.

In the forestry literature, Quantitative Structure Modelling (QSM) has been used to model complex tree structures of living trees, from point cloud data (Hackenberg et al., 2014). This approach could offer an improved way of monitoring wood volume for discrete trees, from the point of living on the floodplain to being incorporated into the active channel. A QSM is a topological ordered structure of building blocks, with cylinders being used for tree modelling, capable of modelling highly accurate cylindrical tree models from terrestrial LiDAR point clouds. A number of workers have developed and applied software such as 'Simpletree' (Hackenberg et al., 2014; Hackenberg, Wassenberg, et al., 2015), to produce accurate models of the branching structure of standing trees, with particular benefits for the estimation of biomass within forests (Demol et al., 2022; Fan et al., 2020; Gonzalez de Tanago et al., 2018; Stovall, Anderson-Teixeira, & Shugart, 2018). This approach has yet to be applied to assessing large wood in rivers and provides an opportunity to assess changes in both tree complexity in terms of branching structure and volume.

The primary objective of this study is to develop a rapid methodology to streamline the process of characterising the complexity of wood branching remotely, thus reducing the time required for in situ manual surveys. Complexity-related parameters may serve as proxies for mechanical fragmentation. We explore the use of photo interpretation as a potential solution for this purpose, which also offers the advantage of being applicable to an existing image bank. The secondary objective is to establish a methodology using terrestrial LiDAR to assess wood volume, which cannot be obtained through photo interpretation alone. Additionally, LiDAR serves as a basis for comparing complexity measures obtained from photo interpretation, enabling us to determine whether it is possible to establish a relationship between complexity metrics and volume. These two methods are then tested on a relatively small sample size, but one that is representative of the study site, in order to evaluate wood fragmentation during its early stages, specifically within the first 2 years after recruitment into the river channel. Information on newly introduced wood pieces, which are monitored over 3 years, is rare and difficult to obtain. To address this challenge, we utilise RFID tracking (Radio Frequency Identification) to monitor newly introduced trees. This allows us to gain insights into the shape evolution of wood pieces and to explore the correlation between residence time and shape. RFID tagging enables the marking of trees and wood pieces, facilitating their monitoring and displacement tracking. Each individual is assigned a unique ID and can be located using an antenna following flood events.

2 | STUDY SITE, MATERIAL AND METHODS

2.1 | Study site

The Allier River in France was selected for studying wood fragmentation, owing to its consistent wood recruitment through bank erosion and active channel shifting. Originating at 1485 m altitude, it drains a catchment area of 14,400 km^2, and flows for 410 km before joining the Loire River at an altitude of 140 m (Figure 1a,b). The study area is situated within the Val d'Allier Natural National Reserve (altitude ~220 m), characterised by a mean channel width of 60 m (sd = 15) and an average annual erosion rate of between 0.2 and 0.9 ha/km/year (between 2009 and 2020). The surveyed wood pieces all come from within 10 km upstream of the Châtel-de-Neuvre gauging station. The hydrograph shows a strong seasonal pattern: the mean annual discharge at Châtel-de-Neuvre where the Allier drains a catchment area of 12,430 km^2, is 114 m^3/s, with Q_2 (2-year return period) and Q_{10} (10-year return period) of 560 and 940 m^3/s, respectively.

2.2 | Imagery based data and method to evaluate wood fragmentation

2.2.1 | Sample description and data acquisition

In total, a sample size of 31 trees was used to develop an easily applicable, cheap and fast method to study wood fragmentation over time (Table 1). Amongst this tree sample, 22 trees were measured once, five trees were monitored twice and four of the trees were measured three times. The trees were monitored using active RFID tags between 2020 and 2022 and their recruitment date (time of entry into the river) is known. Therefore, physical wood fragmentation characteristics of the early stage (first 3 years) can be linked to the residence time spent within the river corridor. Figure 2 shows the flow conditions that triggered recruitment and during the monitoring period. The wood pieces analysed in this study are qualified by some of their physical characteristics. Their size varies widely (from 1.2 to 30-m in length) as does their morphological complexity.

For photo-interpretation, photographs were captured employing a digital camera of 14 MP, from various viewpoints when it was possible, however, there was no consistency between image-overlapping. Ten trees were photographed following their recruitment, implying that they were exposed to one flooding period. The residence time of 1 year is assigned to this group. Twelve trees were subjected to two high flow periods (residence time: 2 years), while 5 trees were exposed to three high flow periods (residence time: 3 years). Three trees were monitored twice, with no identifiable recruitment time. They are categorized as "unknown1" (for the first year of monitoring) and "unknown2" (for the second year of monitoring) classes.

Eleven trees from the 31 samples were characterised while standing (living), allowing an initial state to be described as follows. Although we had images of several trees before they fell into the river (stage 0), these images could not be used to obtain useful parameters to determine wood fragmentation because of the presence of leaves. However, it is crucial to determine the initial characteristics of our sample in order to be able to quantify changes. Obtaining adequate images of a standing tree, where the entire tree is visible with exploitable resolution, is very difficult from ground level. Therefore, to describe the trees before fragmentation caused by the erosive action of floods and temporal degradation, we took drone images of these standing trees in the winter of 2022 in the same area where most of the recently entered trees (1 year of residence time) originated (Table 1). We flew the drone (DJI Mavic 2 pro, 20 MP camera) at a fixed distance from the tree and with the camera pointing horizontally and took multiple images to cover the entire tree from top to bottom (i.e. flying parallel to the tree). The images had ~50% overlap and were stitched together for analysis.

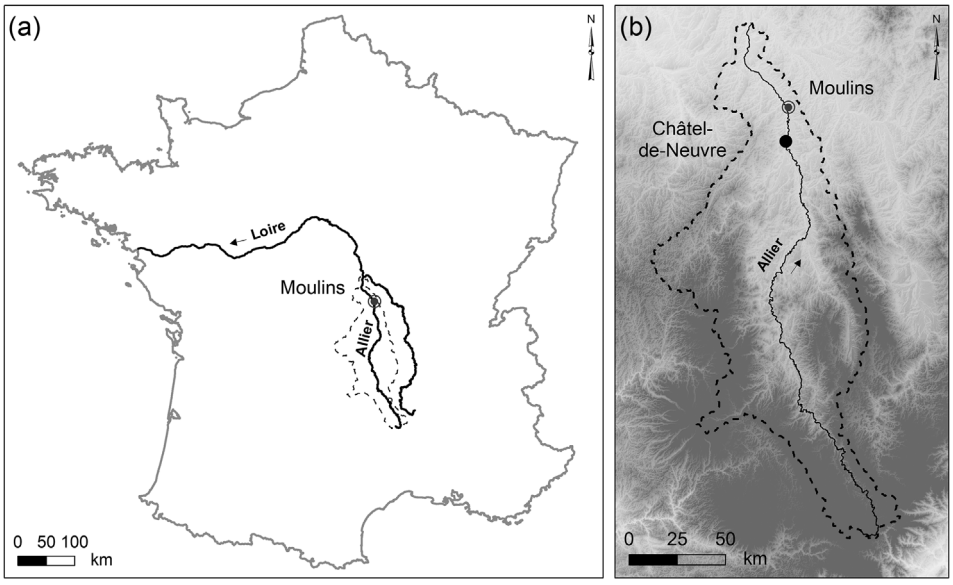

FIGURE 1 (a) Location of the Allier River course in France and its catchment area (dotted line), (b) the catchment area of the Allier River and the village of Châtel-de-Neuvre, located in the centre of the study area.

TABLE 1 Description of wood samples used for photo-interpretation and terrestrial laser scanning analysis. Residence time 0 represents standing (live) trees.

ID	Date of scan	Residence time	Moved	Photo-interpretation	LiDAR	Survey type	Used to describe stage 0
074AB8	2020	1	Yes	Yes	Yes	Both	No
	2021	2	Yes	Yes	Yes	Both	No
	2022	3	No	Yes	Yes	Both	No
074B55	2020	1	Yes	Yes	Yes	Both	No
	2021	2	No	no	Yes	LiDAR	No
	2022	3	No	Yes	Yes	Both	No
074B2B	2020	unknown1	No	Yes	Yes	Both	No
	2021	unknown2	Yes	Yes	Yes	Both	No
074B2A	2020	unknown1	No	Yes	Yes	Both	No
	2022	unknown2	No	Yes	Yes	Both	No
074AA9	2020	1	Yes	Yes	Yes	Both	No
	2021	2	No	Yes	No	Photo	No
	2022	3	Few meters	Yes	Yes	Both	No
074ACC	2020	1	Yes	Yes	Yes	Both	No
	2021	2	No	Yes	Yes	Both	No
	2022	3	No	Yes	Yes	Both	No
074B33	2020	1	Yes	Yes	Yes	Both	No
	2021	2	No	Yes	Yes	Both	No
	2022	3	Few meters	Yes	Yes	Both	No
074B07	2020	unknown1	Yes	Yes	Yes	Both	No
	2022	unknown2	No	Yes	Yes	Both	No
074AE8	2020	0	-	No	Yes	LiDAR	No
	2022	2	Yes	Yes	Yes	Both	No
074A8F	2020	0	-	No	Yes	LiDAR	No
	2022	2	Yes	Yes	No	Photo	No
074B3C	2022	2	Yes	Yes	Yes	Both	No
074ABC	2021	1	Yes	Yes	No	Photo	No
	2022	2	No	Yes	No	Photo	No
074ABE	2022	2	Yes	Yes	No	Photo	No
074ACB	2020	1	Yes	Yes	No	Photo	No
074 AD1	2020	1	Yes	Yes	No	Photo	No
074 AD5	2022	2	Yes	Yes	No	Photo	No
074AEA	2020	1	Yes	Yes	No	Photo	No
074B1A	2022	2	Yes	Yes	No	Photo	No
074B29	2020	1	Yes	Yes	No	Photo	No
074C14	2022	2	Yes	Yes	No	Photo	No
084B43	2022	0	-	Yes	No	Photo	Yes
084B46	2022	0	-	Yes	No	Photo	Yes
084B4F	2022	0	-	Yes	No	Photo	Yes
084B64	2022	0	-	Yes	No	Photo	Yes
084B6E	2022	0	-	Yes	No	Photo	Yes
084B72	2022	0	-	Yes	No	Photo	Yes
084B80	2022	0	-	Yes	No	Photo	Yes
084BA4	2022	0	-	Yes	No	Photo	Yes
084BB5	2022	0	-	Yes	No	Photo	Yes
084 BC1	2022	0	-	Yes	No	Photo	Yes
084C49	2022	0	-	Yes	No	Photo	Yes

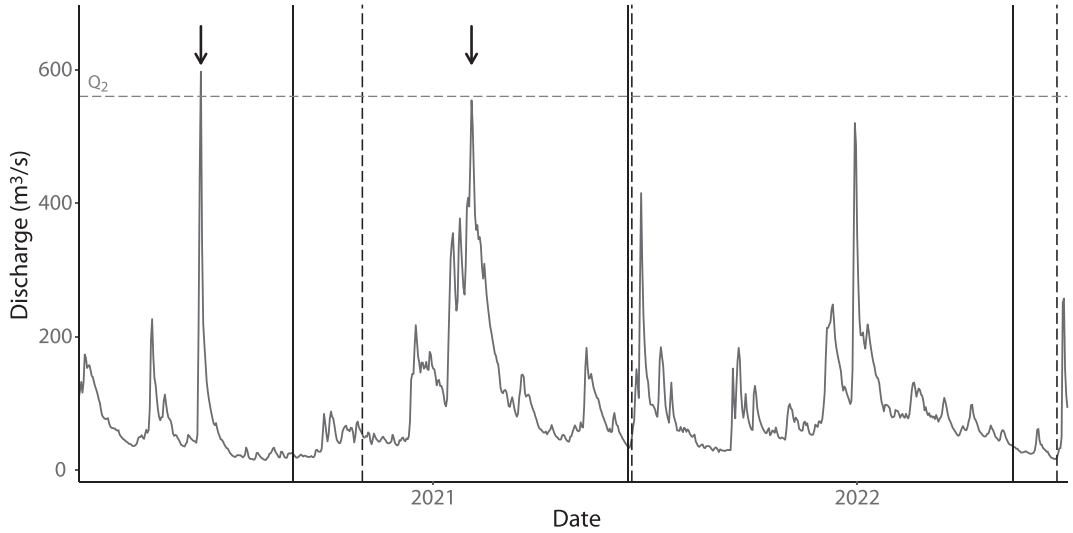

FIGURE 2 Hydrological conditions at Châtel-de-Neuvre showing the mean daily discharge. Images for photo-interpretation were taken on dates indicated by vertical solid lines, and terrestrial LiDAR acquisitions are indicated by vertical dashed lines. The arrow indicates wood recruitment by lateral erosion.

TABLE 2 Metrics obtained by photo-interpretation and LiDAR methodologies. Field measurements for ground truth data are also indicated.

Metrics	Definition	Method
Horton-Strahler branch order	Ordering starting from the finest branches (equal to order of 1) leading toward the main trunk. The order number increases when two branches of equal order join.	Photo-interpretation; Ground truth
Branching complexity	$\sum Horton\ branch\ order_n \times Number\ of\ segment_n$	Photo-interpretation; Ground truth
Branch order	Counted from the trunk up to the tips. At each branch junction the branch order of side branches is increased by 1.	LiDAR
Reverse branch order	Counted from the tips to the trunk. When two segments join, their order must be summed to obtain the order of the following segment.	LiDAR
Cylinder radius	Radius of circles fitted along branches	LiDAR
Volume	Total summed volume of cylinders	LiDAR
Length	Total summed length of cylinder model	LiDAR

2.2.2 | Photo-interpretation using GIS: order and branching complexity

The images were imported into Qgis software for interpretation. Initially, the branch order of each tree was calculated for every year in which images were available. The branch order was determined from the tips to the trunk, using the stream order style being analogous to the Horton system developed by Strahler (Horton, 1932; Strahler, 1957). This system was previously employed for river network analysis. We begin by assigning the order 1 to the finest branches. When two first order segments join, they form a second order segment. Lower order segments joining a higher order segment do not change the order of the higher segment. Using this ordination method on trees, Horton (1932) and Järvelä (2004) observed a consistent morphometric ratio between orders in terms of the volume or length of branches. This method can be used to explore the relationship between a tree branching complexity and its overall volume or length, as well as to quantitatively characterise the tree structure and evolution under different processes such as residence time, accumulation, and transport. After assigning orders to each branch and segment, we calculated a branching complexity index. Our metric for branching complexity was determined by (i) multiplying the rank of a branch/segment by the number of branches at that rank and (ii) by summing the products obtained in step (i) (Table 2).

2.3 | Fragmentation rate quantification using LiDAR

2.3.1 | Large wood scanning using terrestrial LiDAR

Terrestrial LiDAR analysis concentrated on changes in the structure of nine dead and two living trees, in response to both in situ degradation or transport conditions during observed floods. We used repeat-survey terrestrial LiDAR to produce accurate three-dimensional point clouds of several trees over a two-year period, encompassing two winter high flow periods. Three field surveys took place in November 2020, June 2021 and June 2022. Four trees were scanned on three occasions, five of the trees scanned twice and two of them only once. These trees represent a subset of the 31 trees analysed through photo-interpretation, as indicated in Table 1.

Two of the trees were scanned while still standing on the edge of the bank, thus the residence time of 0 was associated, five trees had a residence time of 1 year, six were characterised by a residence time of 2 years, and five trees by a residence time of 3 years. Three of the trees for which the residence time is unknown were monitored two times. Beside the two standing trees, the rest of the trees were scanned on exposed bar surfaces, typically positioned on their side. Scanned trees were usually isolated, however occasionally two trees would be in contact with each other. Trees were scanned during low flow conditions using a Topcon GLS2000 LiDAR (point accuracy of 3.5 mm at 1–150 m), with typically between four and eight scans per tree. It was essential to try to maximise the point coverage of the tree surface and minimise shadow. Scans were merged in Topcon Scanmaster software, using a series of tie-points located around each tree, which were also surveyed using a Trimble GNSS, to allow geo-referencing. Point clouds were then imported into CloudCompare (Brodu & Lague, 2012), and a manual denoising process was conducted whereby the points for each tree were manually extracted by cutting out unwanted areas of the bar surface or adjacent dead wood not part of the tree of interest.

2.3.2 | From point cloud to wood fragmentation assessment

We applied QSM to the point clouds using an open source tool "SimpleTree" (Hackenberg, Spiecker, et al., 2015, https://computree.onf.fr). Hackenberg, Wassenberg, et al.'s (2015) approach requires a terrestrial LiDAR point cloud. Prior to importing data into Simpletree, the coordinates for each tree point cloud were translated/rotated so that the tree was in an upright position along the z plane. Data was imported to Simpletree as a *.las* file. The QSM method uses spheres to follow the complete branching structure of the tree. The spheres' surfaces cut the tree point cloud, resulting in spatially unconnected sub-point-clouds representing the cross-section areas of the branches. Into these sub point clouds circles are fitted and their radii are used for the preliminary fitted cylinders. The cylinders are enhanced with a non-linear least square fitting routine. Hackenberg, Wassenberg, et al. (2015) demonstrate that the resulting cylinder models fit the point clouds very well, covering 99% of the tree and a submillimetre quality fit accuracy. However, problems with occlusion can occur while scanning trees in the field (e.g., Hackenberg, Wassenberg, et al., 2015), or points containing essential information can be lost during the denoising process, resulting in data gaps over portions of branches or the trunk. During the Simpletree modelling process, some branches or twigs may not be modelled properly as the cylinder ends at occlusion gaps, or other areas that still contain noise points can suffer from cylinder overestimation.

The model output from Simpletree provides some useful information that may be applied to assess wood fragmentation through debranching, including volume and length for each modelled cylinder, and measures of complexity namely branch order and reverse branch order (Table 2, Figure 3). In Simpletree, the branch order is counted from the trunk up to the tips. The trunk is initialized with branch order 0. Branches, major branches as well as shoots, splitting from the trunk have the branch order 1. At each branch junction the branch order of side branches is increased by 1 (Hackenberg, 2019). The reverse branch order of a cylinder denotes the maximal number

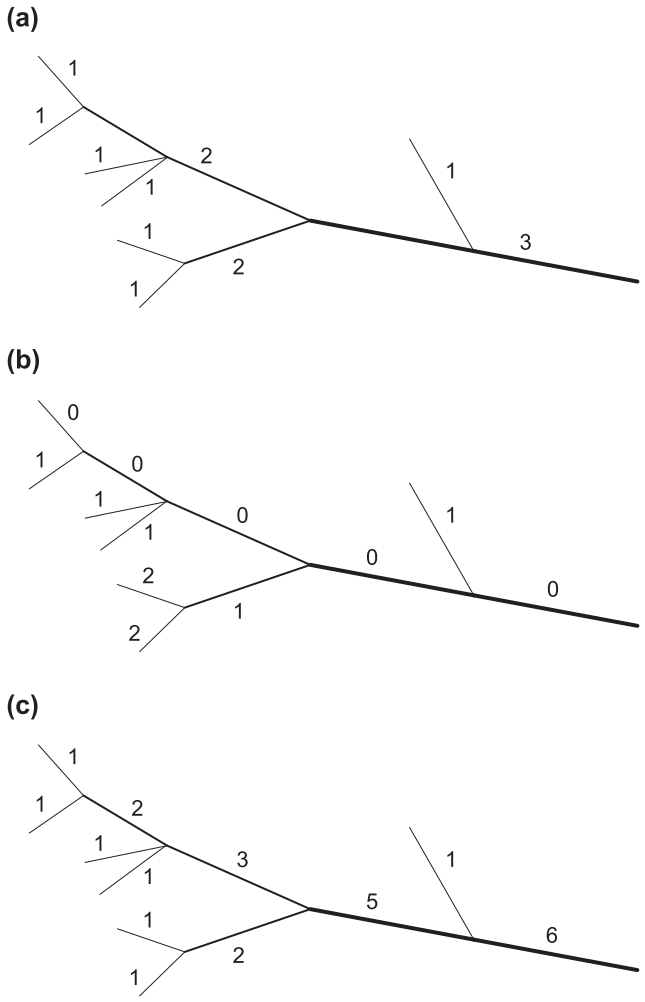

FIGURE 3 Illustration of ordering computation for A) Horton–Strahler branch order, B) Simpletree branch order, C) Simpletree reverse branch order.

of branching splits of the sub-branch growing out of the segment, with the trunk considered as the initial junction (Hackenberg, Disney, & Bontemps, 2022). The reverse branch order is counted from the tips to the trunk. If we apply the concept of ordering, the first order is assigned to the finest branches. When two segments join, their order must be summed to obtain the order of the following segment.

2.4 | Error evaluation using ground truth data and statistical analysis

Four of the most complex trees (i.e., with the highest variability in branch order) analysed by photo-interpretation were selected and their branching complexity calculated in the field. Each tree has a residence time of 3 years. The aim of these independent field measurements was to compare them with photo-interpretation results and to estimate potential methodological biases.

Forestry log scaler volumes were obtained for five trees in 2020 enabling an order of magnitude comparison with terrestrial LiDAR volumes.

Using R software (R Core Team, 2022), a Kruskal–Wallis analysis of variance on ranks was performed on branching complexity, to

determine whether their distribution yielded statistical differences between residence time groups. In the event of a significant outcome (p value ≤0.05), post hoc pairwise multiple comparisons were completed. The Wilcoxon test with Bonferroni p-value correction for multiple paired tests was used.

3 | RESULTS

3.1 | Imagery based method to evaluate wood fragmentation

3.1.1 | Branching complexity and wood fragmentation

The mean (and the median) of branching complexity shows a decreasing trend from 484.2 (365) to 43 (42) with increasing residence time from 0 to 3 years (Figure 4a, Table 3, Table 4). The median decreases by 54%, 62% and then by 34% respectively. For wood pieces with an indeterminate residence time, the branching complexity also decreases further from 34 (30) to 14 (15). There is a significant difference between the 0 and 1 year residence time groups and the 1 and 2 year groups (Figure 4a). Branching complexity values are more dispersed within the group of the standing trees (residence time 0) and strongly reduced for the group with a residence time of 3 years and more. During the first 2 years, wood fragmentation is much faster than in the later stage and accounts for 83% of the reduction of branching complexity. The median of the number of first order segments decreases with increasing residence time by 56%, 57%, 39%, 21% and 53% (Figure 4b). The median Horton-Strahler tree order (i.e., the highest order per tree) is not sensitive enough to differentiate the groups according to residence time, although it shows an overall decreasing tendency with increasing residence time (the medians per group are respectively: 4, 4, 3, 3, 3, 2).

3.1.2 | Error evaluation using ground truth data

Field measurements of branching complexity and segment number show that photo-interpretation tends to underestimate these parameters by at least 42% (Table 5). The error for the most complex tree is higher and amounts to 71%. The RMSE of branching complexity ranges from 26 to 196. The underestimation also concerns the order level for two out of four trees (Table 5).

3.2 | Wood fragmentation assessment using LiDAR

3.2.1 | Point cloud and cylinder fit

Table 6 demonstrates details of the 11 trees that were scanned. Point coverage typically was 792,861 points per tree, equivalent to 4,650 pts/m^2 on average (Table 6). Many trees were scanned on their side, resting on bar surfaces, where some branches were partly buried underneath bar surface sediment, hence introducing minor occlusion problems. One further complication in the comparisons result from local changes in bed elevation around the tree between floods caused by local scour and fill of bed sediment around branches. Where trees had been transported and the position of the tree had changed this also resulted in variations in point coverage over the tree between surveys.

Figure 5 shows point clouds for four out of the 11 sampled trees alongside cylinder models produced using Simpletree, and fragmentation over the study period. In general, the cylinder models resemble the point clouds extremely well. To investigate the success of the cylinder modelling further we compared the point cloud to the cylinder surface. Summary statistics are shown in Table 6, where typically it can be seen that points on average were <3 cm from the modelled cylinder surface. There is however substantial variability between trees and surveys.

3.2.2 | Wood fragmentation evolution using LiDAR data

Temporal fragmentation is visually apparent for all sampled trees (e.g., Figure 5). Summary statistics extracted from the cylinder models are shown in Table 7 for each tree. Reductions in volume and length can all be seen, with one exception (074B33), where the volume appears to increase between 2021 and 2022. This is likely to be an

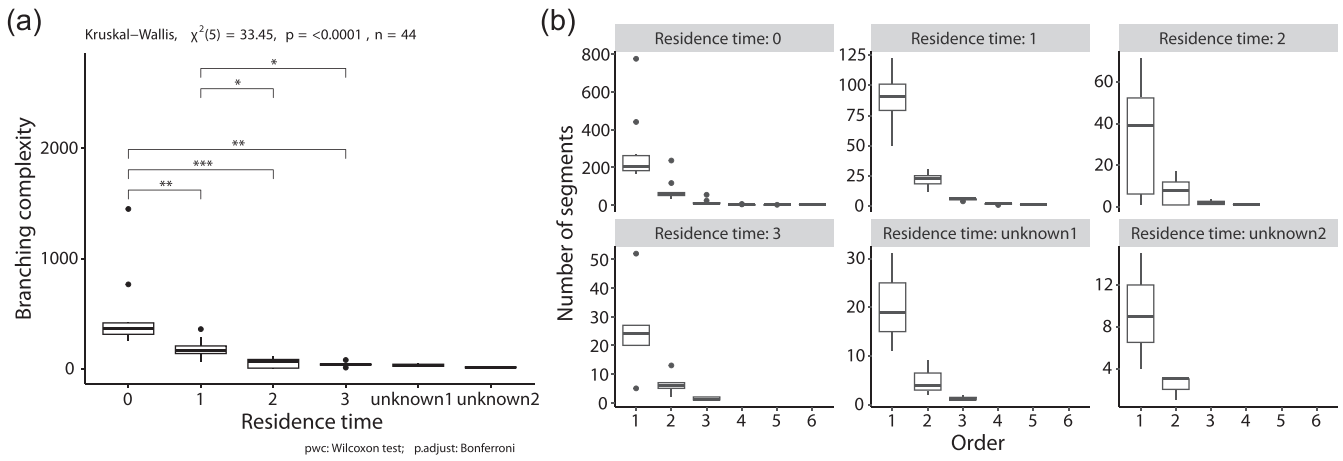

FIGURE 4 (a) Branching complexity in relation to residence time; (b) segment number according to order and residence time.

TABLE 3 Photo-interpretation derived branching complexity and segment number.

ID	Date	Residence time	Order	Branching complexity	Segment number
074A8F	2022	2	1	1	1
074AA9	2020	1	4	213	162
074AA9	2021	2	4	84	65
074AA9	2022	3	3	12	8
074AB8	2020	1	5	163	118
074AB8	2021	2	4	113	86
074AB8	2022	3	3	81	66
074ABC	2021	1	3	159	125
074ABC	2022	2	3	91	70
074ABE	2022	2	2	4	3
074ACB	2020	1	3	61	49
074ACC	2020	1	4	133	101
074ACC	2021	2	4	74	57
074ACC	2022	3	3	42	32
074 AD1	2020	1	4	195	147
074 AD5	2022	2	3	80	75
074AE8	2022	2	2	8	7
074AEA	2020	1	4	290	212
074B1A	2022	2	4	94	71
074B29	2020	1	5	361	268
074B33	2020	1	3	89	67
074B33	2021	2	3	53	43
074B33	2022	3	3	44	35
074B3C	2022	2	2	9	8
074B55	2020	1	4	175	134
074B55	2022	3	3	36	27
074C14	2022	2	2	4	3
084B43	2022	0	4	365	287
084B46	2022	0	6	1,451	1,074
084B4F	2022	0	4	400	294
084B64	2022	0	4	345	264
084B6E	2022	0	5	409	326
084B72	2022	0	5	336	253
084B80	2022	0	4	426	342
084BA4	2022	0	5	767	586
084BB5	2022	0	4	258	214
084 BC1	2022	0	4	277	216
084C49	2022	0	4	292	232
074B2A	2020	unknown1	3	18	14
074B2A	2022	unknown2	2	6	5
074B2B	2020	unknown1	3	55	42
074B2B	2021	unknown2	2	15	12
074B07	2020	unknown1	3	30	24
074B07	2022	unknown2	2	21	18

issue of hidden branches in 2021 because of sediment burial. Most trees showed a reduction in branch order. Some however kept the same ordering. Most of the results for the reverse branch order statistic show a reduction.

The median of each of the four terrestrial LiDAR-derived wood fragmentation proxies shows a decreasing trend with residence time, except for reverse branching order between state 3 and unknown1 and the volume between states 2 and 3 (Figure 6, Table 8). However,

TABLE 4 Branching complexity and 1st order segment number statistics according to residence time measured by photo-interpretation.

		Branching complexity				1st order segment number			
Residence time	Sample size	Median	Mean	25% quantile	75% quantile	Median	Mean	25% quantile	75% quantile
0	11	365.0	484.2	314.0	417.3	206.0	278.8	182.5	262.0
1	10	169.0	183.9	139.5	208.5	90.5	88.8	79.3	101.0
2	12	63.5	51.3	7.0	85.8	39.0	33.4	6.3	52.3
3	5	42.0	43.0	36.0	44.0	24.0	25.6	20.0	27.0
Unknown1	3	30.0	34.3	24.0	42.5	19.0	20.3	15.0	25.0
Unknown1	3	15.0	14.0	10.5	18.0	9.0	9.3	6.5	12.0

TABLE 5 Branching complexity and order statistics of four trees of tree-year residence time comparing photo-interpretation and field measurements.

	Branching complexity				Order	
Sample	Photo-interpretation	Field	RMSE	Underestimation (%)	Photo-interpretation	Field
074AB8	81	277	196	71	3	5
074ACC	42	86	44	51	3	4
074B33	44	83	39	47	3	3
074B55	36	62	26	42	3	3

TABLE 6 LiDAR scan and cylinder model accuracy statistics.

			LiDAR scan statistics and cylinder model accuracy				
ID	Date of scan	Residence time	Number of scans	Number of points in cloud	Point spacing (pts/m^2)	Mean point distance to model (m)	Std dev
074AB8	2020	1	8	1,163,477	4,379	0.034	0.124
	2021	2	5	1,316,820	7,511	0.014	0.037
	2022	3	6	2,767,767	23,636	0.019	0.048
074B55	2020	1	8	1,145,938	3,460	0.011	0.047
	2021	2	7	603,472	2,492	0.019	0.061
	2022	3	10	853,700	8,557	0.026	0.065
074B2B	2020	unknown1	4	82,682	4,957	0.008	0.022
	2021	unknown2	3	167,687	22,122	0.005	0.018
074B2A	2020	unknown1	4	125,511	2,843	0.003	0.024
	2022	unknown2	2	573,975	19,923	0.001	0.013
074AA9	2020	1	4	434,277	1744	0.011	0.052
	2022	3	6	769,905	7,785	0.006	0.035
074ACC	2020	1	8	426,199	2,827	0.049	0.076
	2021	2	7	577,552	4,645	0.016	0.074
	2022	3	10	297,640	3,327	0.100	0.387
074B33	2020	1	8	2,004,461	6,762	0.030	0.119
	2021	2	7	827,667	3,411	0.023	0.128
	2022	3	10	685,384	3,141	0.114	0.260
074B07	2020	unknown1	8	418,983	2,712	0.009	0.039
	2022	unknown2	4	843,005	8,852	0.007	0.031
074AE8	2020	0	5	555,470	568	0.104	0.329
	2022	2	6	531,041	15,725	0.005	0.024
074A8F	2020	0	5	1,716,956	102,139	0.021	0.061
074B3C	2022	2	6	139,097	9,003	0.059	0.181

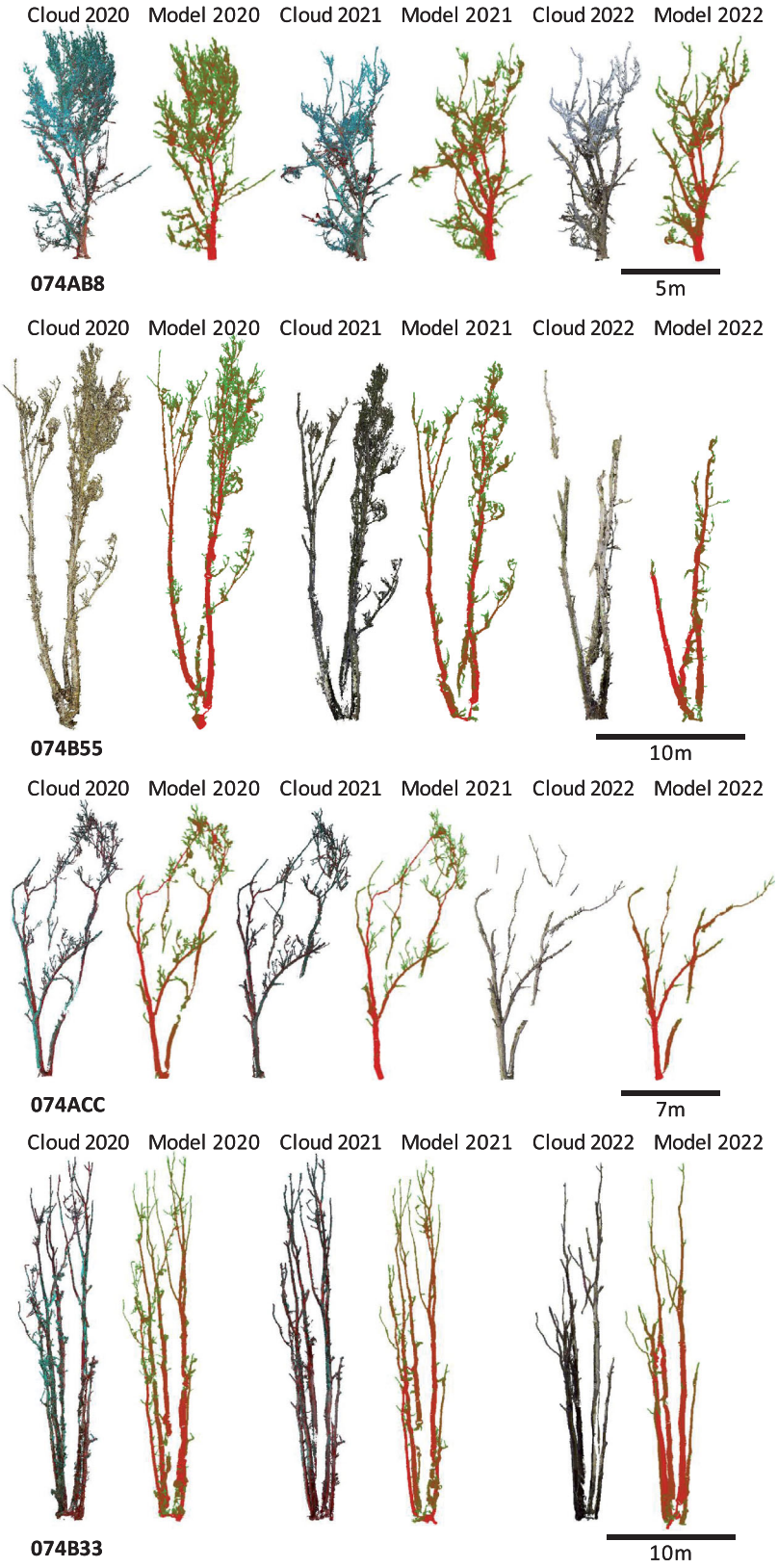

FIGURE 5 Comparisons of point clouds and cylinder models for four trees (074AB8, 074B55, 074ACC, 074B33), showing fragmentation over the study duration.

the sample size is too small to test for significant differences. Length has the largest relative loss compared with the residence time group T^{-1} until 3-year residence time group, i.e., 69%, 55%, 54% and 56%. Length decreases by 43% between the two unknown residence time classes. The median wood volume decreases from 16.1 m^3 to 0.8 m^3 and the relative losses are 61%, 45%, −15%, 70% and 36% for each of the residence time classes. The variability of the length decreases strongly with time compared with the volume.

Another useful measure of complexity that can be retrieved from the Simpletree output is the cylinder radius. The hypothesis here is that as trees gradually fragment over time, as branches gradually break off the tree, the relative proportion of cylinders with a small radius will reduce. Table 7 shows the temporal change in the population distribution of cylinder radii for each of the tree cylinder models, and presents summary statistics for the curves. Cylinder radii population curves are also shown in Figure 7, showing changes for

TABLE 7 Terrestrial LiDAR-derived volume, length, complexity measures and cylinder modelling statistics for each scanned tree.

ID	Date	Volume (m^3)	Length (m)	Branch order	Reverse branch order	Tree radii population (m)				Forestry log scaler volume
						Skewness	Kurtosis	Mean	Median	
074A8F	2020	3.1	1730.0	5	155	2.4	12.2	0.02	0.01	
074AA9	2020	6.3	704.1	6	83	5.2	48.7	0.03	0.02	
074AA9	2022	5.1	53.9	2	16	0.8	4.3	0.13	0.12	
074AB8	2020	6.1	568.8	5	79	2.1	10.8	0.04	0.04	7
074AB8	2021	4.1	318.9	5	36	2.5	12.1	0.05	0.03	
074AB8	2022	3.4	190.9	5	25	2.5	12.2	0.05	0.04	
074ACC	2020	4.0	271.5	4	49	2.3	10.4	0.05	0.04	3
074ACC	2021	2.9	260.7	4	71	3.5	22.3	0.04	0.03	
074ACC	2022	2.9	81.1	3	20	1.6	6.9	0.08	0.06	
074AE8	2020	29.2	1977.9	6	77	2.2	12.8	0.05	0.04	
074AE8	2022	2.8	15.5	1	2	−1.0	3.5	0.21	0.23	
074B07	2020	6.6	128.3	3	25	1.3	5.9	0.09	0.07	4
074B07	2022	4.1	71.7	3	26	0.7	2.9	0.11	0.10	
074B2A	2020	1.2	52.0	2	16	1.2	4.0	0.06	0.05	
074B2A	2022	0.8	29.7	2	7	0.7	2.6	0.07	0.06	
074B2B	2020	0.2	48.5	3	27	1.8	7.4	0.03	0.03	
074B2B	2021	0.1	19.0	1	5	3.3	25.5	0.03	0.03	
074B33	2020	10.9	395.1	4	61	2.2	9.3	0.06	0.04	10
074B33	2021	8.4	254.6	4	30	1.4	5.0	0.07	0.06	
074B33	2022	9.5	161.8	3	23	1.0	3.4	0.10	0.08	
074B3C	2022	0.4	19.8	2	10	0.8	3.0	0.06	0.05	
074B55	2020	8.3	697.9	5	72	2.8	14.8	0.04	0.03	4
074B55	2021	7.6	379.8	6	71	1.6	5.9	0.06	0.05	
074B55	2022	4.0	117.4	3	40	1.2	3.7	0.07	0.05	

each tree over the study duration. Results broadly show the expected pattern with greater proportions of larger radius branches found progressively through the three surveys.

Tree 074AA9 shows a shift from a mean branch radius of 0.03 to 0.13 m (+433%) between 2020 and 2022. This significant coarsening, was a consequence of the removal of nearly all the finer branches from the main part of the trunk. Tree 074AB8 shows a shift from a mean branch radius of 0.04 to 0.05 m (+125%) between 2020 and 2022. This tree was transported a considerable distance between 2020 and 2021, and then remained in situ on a bar surface downstream between 2021 and 2022. The tree showed a more gradual loss of finer branches, with the main parts of the trunk remaining intact. Tree 074ACC shows a shift in mean branch radius from 0.05 to 0.08 m (+160%) between 2020 and 2022. This tree was situated adjacent to 074B33 for the first two surveys, and then was isolated, remaining in approximately the same position after 074B33 was transported further down the bar between 2021 and 2022. This tree showed relatively minor loss of smaller branches between 2020 and 2021, and then more significant loss of the smaller branches between 2021 and 2022. Again, the trunk and main branches remain intact. Tree 074AE8 shows a shift in mean branch radius from 0.05 to 0.21 m (+420%) between 2020 and 2022. Tree 074B07 showed a shift in mean branch radius from 0.09 to 0.11 m (+122%) between 2020 and 2022. This tree was transported between these dates, and hence would have been subject to the effects of fluvial processes in addition to weathering in situ. During the first scan, the tree comprised three initial elements to the main trunk, with most minor branches already lost. The 2020 survey revealed further loss of some smaller branches and loss of roughly half of one of the three main trunk elements. Tree 074B2A showed a shift in mean branch radius from 0.06 to 0.07 m (+117%) between 2020 and 2022. This tree already lost most of its small branches in the initial scan, and showed some loss of the coarse branch tips while remaining in situ of the edge of a bar. The mean branch radius for tree 074B2B stayed constant at 0.03 m between 2020 and 2021, despite the 2021 curve showing a very slight coarsening, rather visible on Figure 7, with some loss of finer branches evident when observing the cylinder model. Tree 074B33 showed a shift in mean branch radius from 0.06 to 0.10 m (+167%) between 2020 and 2022. This tree only moved slightly on a bar surface over this period and would have been subject some fluvial, but mainly weathering processes in situ. Observation of the cylinder model shows a gradual loss of finer branch elements. Tree 074B55 showed a shift in mean branch radius of 0.04 to 0.07 m (+175%) between 2020 and 2022. This tree remained on the head of a point bar over the study duration, only showing minor movement, and would have been mainly subject to the effects of weathering processes. Observation of the cylinder models indicates greater loss of smaller branches between 2020 and 2021, and less significant loss in between 2020 and 2021.

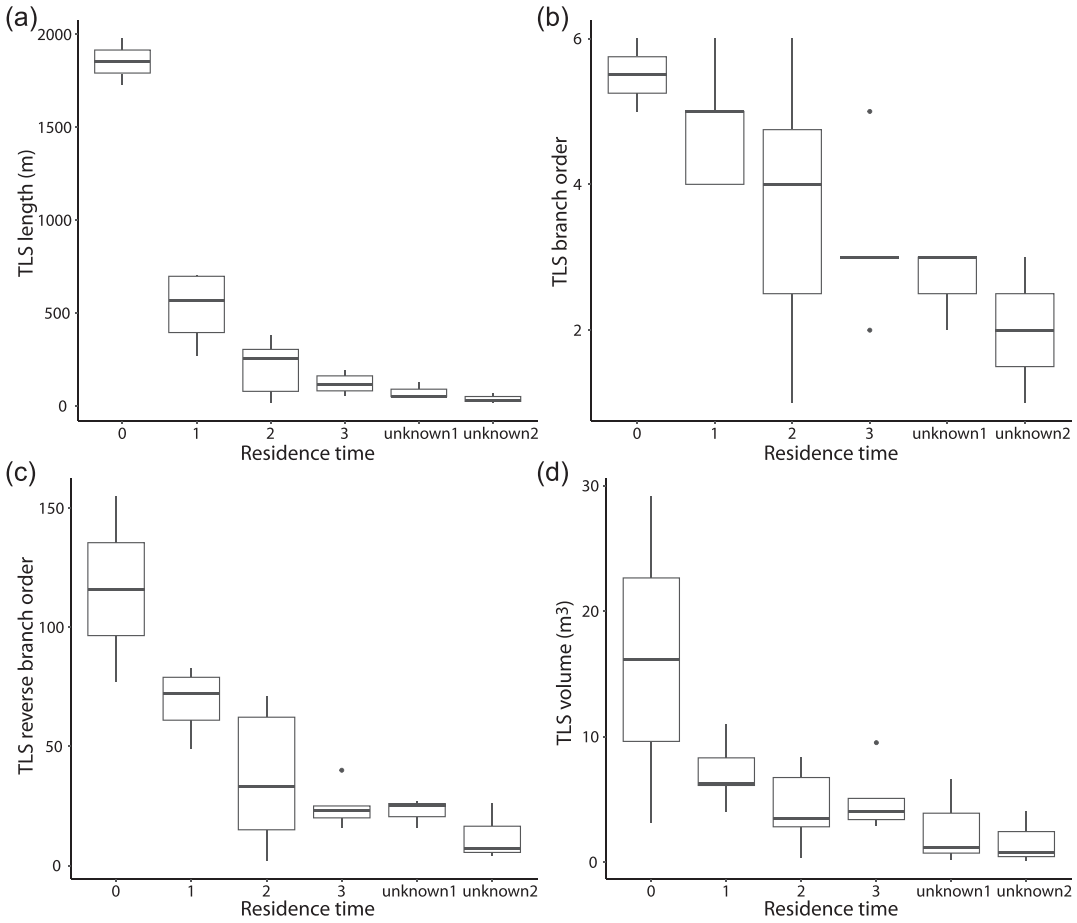

FIGURE 6 Terrestrial LiDAR-derived (TLS) (a) length, (b) branch order, (c) reverse branch order and (d) volume in relation to residence time. The injection time of class "unknown" is not known and corresponds to greater residence time. "Unknown2" represents the same trees as in class 'unknown1" but rescanned one or two years later.

The volumes calculated by Simpletree were close to the forest cubage measurements except for one tree which was greatly overestimated by the terrestrial LiDAR measurements (Table 7).

3.3 | Interrelation of photo-interpretation and LiDAR fragmentation metrics

Figure 8 shows strong correlations between photo-interpretation derived branching complexity and A) Terrestrial LiDAR-derived length ($R^2 = 0.9$), B) Terrestrial LiDAR-derived branch order ($R^2 = 0.78$) and C) Terrestrial LiDAR-derived reverse branch order ($R^2 = 0.78$). However, the correlation between the branching complexity obtained from photo-interpretation and the volume measured by Terrestrial LiDAR (Figure 8d) is not as robust ($R^2 = 0.2$) and seems to highlight two different relationships.

Based on our results, it is not feasible to derive wood volume directly from the image branching complexity metric described above (Figure 8d). Figure 8d depicts a division in the point cloud, where the wood pieces with high branching complexity (with numerous fine branches) can be found towards the right-hand side of the figure, indicating an overestimation of branching complexity in relation to the volume. Logically, it may be necessary to use additional wood parameters, such as diameter to develop a complexity metric that correlates with wood volume. Hence, we examined the relationship between wood volume and the subsequent metric:

$$\sqrt[n]{BC} * \text{Diameter} \quad (1)$$

Where n is the maximum order reached and BC is image derived branching complexity. The correlation coefficient is significantly higher in this case ($R^2 = 0.64$) in comparison with the initial branching complexity metric (Figure 9). However, the correlation between the modified branching complexity and the residence time is no longer present.

3.4 | Displacement and fragmentation

Between the three sampling periods, trees were exposed to high flow conditions (Figure 2). Some trees travelled several kilometres between two measurements, others stayed in places, or moved only few meters from their original position (Figure 10). Both branching complexity (Figure 10a) and volume (Figure 10b) decreased, regardless of their displacement type or stability. There was only one exception, 074B33 which increased its volume as explained above, but this is clearly related to the difficulty to scanning partially buried wood pieces.

TABLE 8 Terrestrial LiDAR-derived length, branch order, reverse branch order and volume statistics according to residence time.

Residence time	Sample size	Length (m)				Branch order				Reverse branch order				Volume (m^3)			
		Median	Mean	25% quantile	75% quantile	Median	Mean	25% quantile	75% quantile	Median	Mean	25% quantile	75% quantile	Median	Mean	25% quantile	75% quantile
0	2	1854.0	1854.0	1792.0	1915.9	5.5	5.5	5.3	5.8	116.0	116.0	96.5	135.5	16.1	16.1	9.6	22.6
1	5	568.8	527.7	395.1	697.9	5.0	4.8	4.0	5.0	72.0	68.8	61.0	79.0	6.3	7.1	6.1	8.3
2	6	257.7	208.2	78.5	304.4	4.0	3.7	2.5	4.8	33.0	36.7	15.0	62.3	3.5	4.4	2.8	6.7
3	5	117.4	121.0	81.1	161.8	3.0	3.2	3.0	3.0	23.0	24.8	20.0	25.0	4.0	5.0	3.4	5.1
unknown1	3	52.0	76.3	50.3	90.1	3.0	2.7	2.5	3.0	25.0	22.7	20.5	26.0	1.2	2.7	0.7	3.9
unknown2	3	29.7	40.1	24.3	50.7	2.0	2.0	1.5	2.5	7.0	12.7	6.0	16.5	0.8	1.7	0.5	2.4

4 | DISCUSSION

4.1 | Methodological issues and solutions for quantifying wood fragmentation

Photo-interpretation provides a convenient and cost-effective approach to assessing wood fragmentation efficiently. However, the available data set only encompasses a small proportion of the monitored wood pieces, limited to just five pieces with a residence time of 3 years. Thus, enriching this dataset would be a worthwhile endeavour. However, our analysis has some limitations regarding the measured parameters. The limited sensitivity of the order and the significant dispersion of the branching complexity within the early stage of the residence time hinder our ability to use it as a proxy to estimate wood volume. This is because a wood piece with numerous fine branches has a high branching complexity, but the fine branches have a low volume. The presence of many fine branches leads to higher values of branching complexity compared with other trees with similar volumes (data points on the right-hand side of Figure 8d). However, once the fine branches are lost, the relationship between volume and branching complexity follows the trend of other trees (data points on the left-hand side of Figure 8d). Therefore, the second suggested calculation method (Equation 1) removes the disproportionate weight of first-order fine branches and makes the adjustment based on wood size. Branching complexity measures were instead found to be suitable for capturing the general dynamics of morphological change and for linking to terrestrial LiDAR complexity parameters (i.e., length, branch order and reverse branch order). Despite photo-interpretation underestimating complexity compared with ground truth data, there appears to be a relationship between the values, allowing for sample comparison. Since the branching complexity by photo-interpretation is well related to the measured tree volume or length, this underestimation does not hinder the fragmentation analysis. The photo-interpretation method may encounter an issue with operator-dependent variability of results. The complete characterisation of the tree structure is altered because of the limitations of a 2D view and the resolution of the photography. It has been decided to only examine the branches that are clearly visible in the image, excluding smaller and intertwined branches, in order to focus on the overall structure of the tree (which is related to the total volume and length) rather than to fully capture its complexity. Considering the smallest segments of the tree may increase the variability with the actual tree, whereas capturing the global structure reduces the risk of variability. Nonetheless, the threshold for branch consideration is a subjective criterion in the photo-interpretation method. Indicative thresholds could be established by using picture scaling to reduce this subjectivity. Only one observer provided the present values to mitigate observer bias, but an analysis of observer bias is still necessary for comparing other sites or even continuing this field effort. We provide our photos along with the data to facilitate potential future studies to test observer bias or compare results. Automating photo interpretation could extend the database and avoid observer bias. For example, advances in this domain have been made using machine learning to automatically detect wood pieces from aerial imagery (Ruiz-Villanueva et al., 2024). Ideally, with a larger database, a relationship should be established between photo-interpretation derived parameters and terrestrial LiDAR-derived volumes. Consequently,

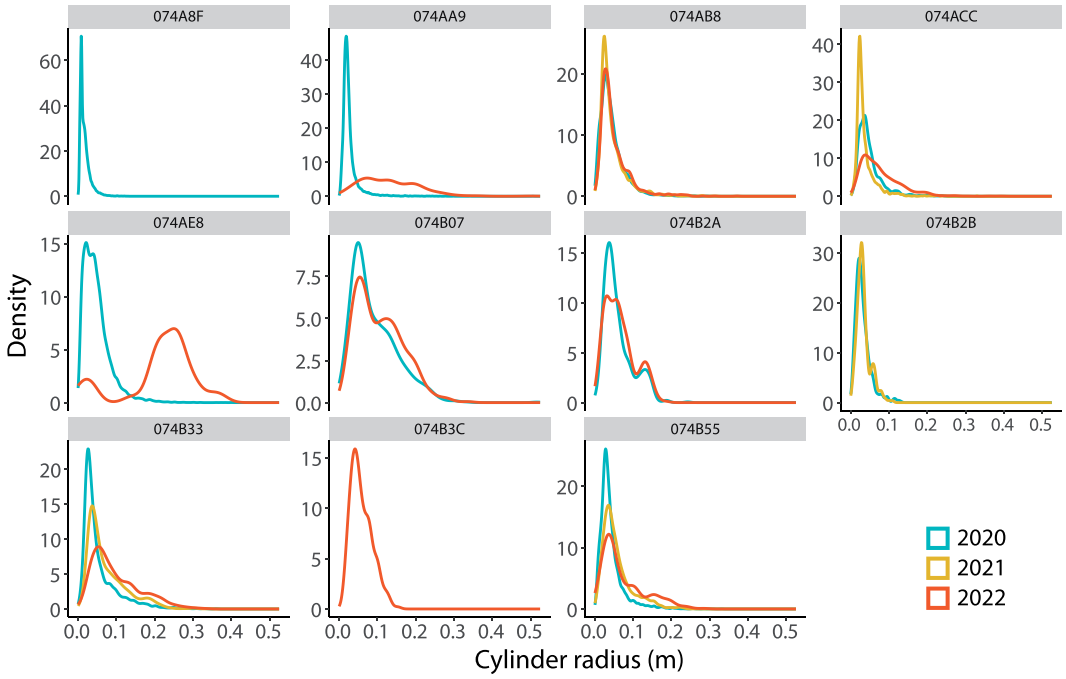

FIGURE 7 Kernel density plots representing changes in population distribution of tree radius derived from cylinder modelling using Simpletree.

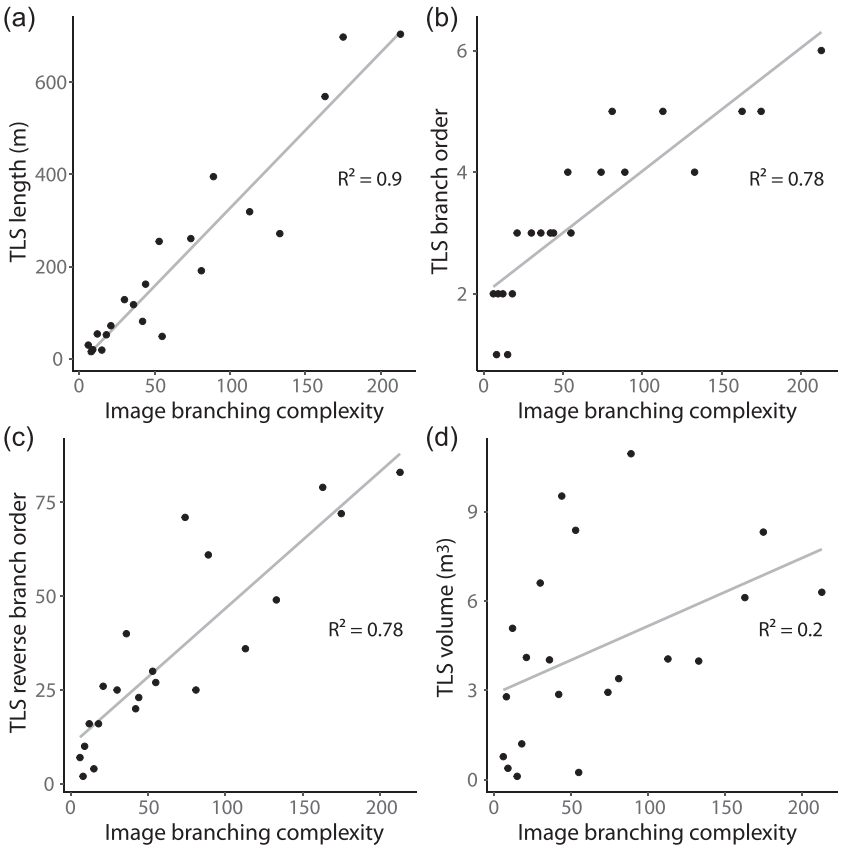

FIGURE 8 Relationship between photo-interpretation derived branching complexity and (a) terrestrial LiDAR-derived length, (b) branch order, (c) reverse branch order and (d) volume.

wood volumes could be derived from photo-interpretation measures alone in the future. Notably, photo-interpretation effectively describes the fragmentation trajectory, which correlates with the reduction in wood volume. If this relationship is confirmed through further observations, photo-interpretation can act as a strong proxy in revealing details about the volume of wood and how it changes over time and space.

Although we did not use photo-interpretation to derive volume and mass estimates, approaches that are able to quantify the full three-dimensional structure of large wood could have advantages over photo-interpretation approaches in this regard. Terrestrial LiDAR provides a solution to obtain a three-dimensional point-cloud of tree structure. Alongside terrestrial LiDAR's advantages, certain limitations are apparent. Conducting data collection and processing is a time-

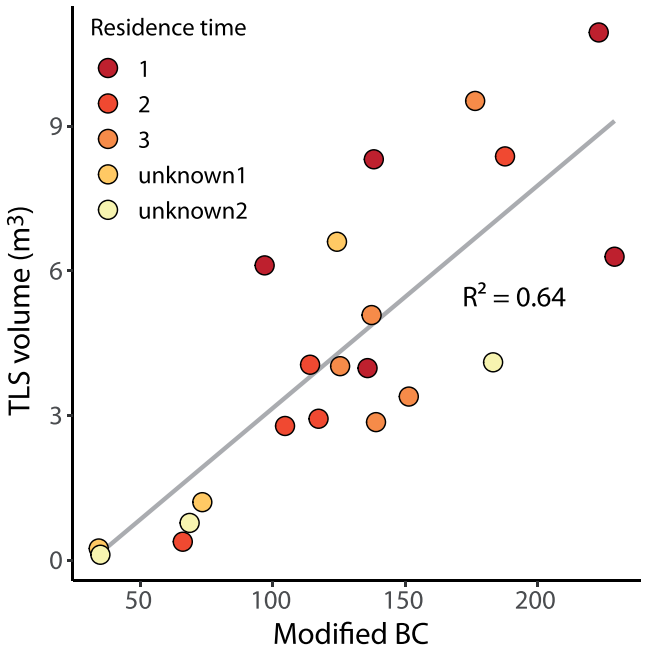

FIGURE 9 Relationship between photo-interpretation derived modified branching complexity and terrestrial LiDAR-derived volume.

consuming task and field logistics prove more challenging than image collection for photo-interpretation. It is important that enough scans are taken to reduce occluded areas, and it is necessary for trees to be exposed above the water surface. Scour and fill around trees on bar surfaces may either expose or hide some branches. In the instance of a branch partially buried, the computation of order is disrupted, unlike photo-interpretation where the observer can virtually connect the unburied parts of the branch. There may also be problems in scanning trees in leaf, for example living trees in the bank edge, however the potential may be overcome through full waveform processing LiDAR. If multiple wood pieces are present within a close proximity, extensive manual cleaning of the point cloud might be necessary. Both photo-interpretation and terrestrial LiDAR measurements may cause slightly inconsistent diachronic outcomes because of the above-mentioned burial process, which can vary in extent from year to year, or because of the variable angle of data collection and our ability to obtain good quality information from the same pieces of wood when, for example, the view is obstructed.

Structure from motion (SfM) photogrammetry may also be used to derive high resolution point clouds for large wood (Spreitzer et al., 2020a), provide data for QSM cylinder modelling, and may offer a lower cost option to using terrestrial LiDAR. However, some studies

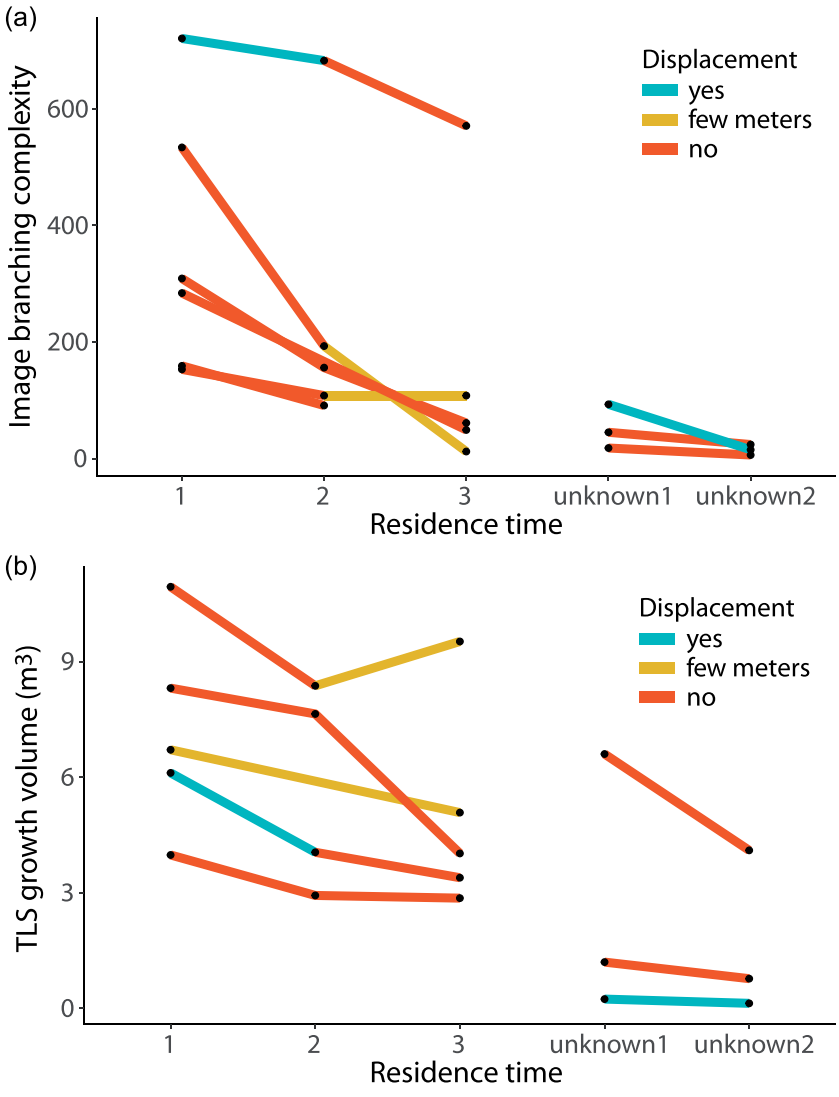

FIGURE 10 (a) Image branching complexity and (b) terrestrial LiDAR-derived volume evolution in time in relation to wood displacement between measurements.

have demonstrated lower accuracy of SfM photogrammetric point clouds for morphology and roughness estimation in gravel-bed rivers (Schwendel & Milan, 2020).

Previous work that has utilised point clouds of large wood in rivers have used meshing algorithms to model wood complexity for large jams. For example, Spreitzer et al. (2019) found Poison Surface Reconstruction using the Pix4D model provided optimum results, when considering wood volume. Through using meshing approaches plus knowing the characteristics of the wood structures, Spreitzer et al. (2020b) were able to calculate porosity through subtracting the 3D geometric volume (3D, geo) from the computed bulk volumes (2.5D or 3D, PSR), providing an assessment of accumulation porosity. We contend that although meshing algorithms may be suitable to assess large wood large jams comprising logs that have lost finer branches (e.g., Spreitzer et al., 2020a), the approach is unable to resolve intricate branching complexity found in trees recently introduced to river channels. For the first time, we demonstrate that QSM cylinder modelling of point clouds successfully resolves this complexity, allowing full quantification of branching structure changes over time as well as the size (length and radius) and volume of the wood.

4.2 | The role of residence time in wood fragmentation

There are relatively few studies on large wood fragmentation. Most of them focus on the length loss and fracturing of wood pieces in the channel, without monitoring the debranching phenomenon or studying the effect of the residence time. For example, both Iroumé, Ruiz-Villanueva, & Picco (2017) and Merten et al. (2013) monitored an impressive number of instrumented wood pieces, but their injection time into the watercourse was unknown. A median fragmentation of between 1 and 4% per year was measured by Iroumé, Ruiz-Villanueva, & Picco (2017), and a size loss of between 5 and 27% over seven years, meanwhile Merten et al. (2013) recorded a mass loss through fragmentation of 7.3% over a one-year period. Here, we measured a mean annual volume reduction of 32% which is much higher compared with these previous studies. Merten et al. (2013) also measured the reduction of mean branching complexity which accounted for 17.73 during the first and 13.62 the second year. This branching complexity range is only comparable with our "unknown2" class (mean: 14) and much lower compared with all other residence time classes (1 year residence time: 184, "unknown1" residence time: 34). Because of disparities in sampling, operators and study period, these values are not very comparable.

A strong correlation between branching complexity and residence time was detected. The first three groups of residence times are clearly differentiated, enabling association of branching complexity ranges with residence time classes. This establishes the possibility of estimating the residence time of wood based on the observed branching complexity in the future. The values for branching complexity exhibited the broadest range within the 0-year class. The rapid decrease of first order segments after recruitment indicates a primary loss of fine branches. This process occurs rapidly in the early stage, reaching more than 50% of the loss within the first year. However, after 2 years of residence, changes in wood geometry become negligible or very slow, suggesting that the skeleton with few main branches is more resistant over time. After a period of 2 years immersed within the fluvial system, the outcome of mechanical fragmentation is no longer a gradual loss of terminal branches, but more pronounced morphological changes, probably due to a fracturing process.

Our field observations also show that fine branches may remain attached to the highest (i.e., furthest from the ground), unsubmerged part of a tree for a longer duration, despite transportation in the river channel. Tree number 074AB8 retained its fine branches for the full 3-year period, and tree number 074ACC retained them for the first 2 years. Consequently, they exhibit higher values of branching complexity when compared with other trees with similar volume (data points on the right side of the Figure 8d). On the other hand, trees 074B55 and 074AA9, which are characterised by the highest branching complexity values, lost their fine branches immediately after the first year. Consequently, in the subsequent years, the relationship between volume and branching complexity followed the trend of the other trees (data points on the left-hand side of the Figure 8d). Taking into consideration the diameter when calculating, and giving a reduced weight to thin branches, which typically lack volume, we have identified a complexity parameter that shows a strong correlation with volume. However, this parameter does not correlate with residence time.

Fine branches detach rapidly from their initial structure and remain highly mobile (with limited storage, representing only 30% of the volume of jams) (Schalko, 2017). It is reasonable to presume that fine branch loss is slowed by the flexibility of fresh branches compared with older, dry branches. Further research is required to examine the variations in branch strength over time and its correlation with weathering conditions, such as wetting-drying cycles and extreme temperatures. In situ or laboratory experiments could help advance these questions by monitoring the biomechanical properties of wood from the moment it enters the river or by using fresh wood. Such research could lead to a better understanding of the evolution of wood shape in response to hydrological constraints. Transported small branches may not pose a significant risk, but they do play an essential role in maintaining the ecological condition of the watercourse and, potentially, in the supply of carbon. It is the element most susceptible to chemical degradation (Merten et al., 2013), an important process in terms of nutrient input. It is also one of the components that accumulates in jams, making these environments rich in ecological diversity.

We analysed wood deposited on alluvial bars and none of the samples were constantly submerged in water or deposited in the alluvial forest. These environmental contexts have the potential to alter debranching and fragmentation processes which were not taken into account in our study. Although beavers were evident at our study sites, there was no sign of their activity in any of the sampled specimens. Our research has focused on branching complexity, but this is clearly not the only factor influencing wood entrainment. For instance, the presence and size of root must also be taken into account (Abbe & Montgomery, 1996; Bisson et al., 1987; Ravazzolo et al., 2022; Welber, Bertoldi, & Tubino, 2013).

Despite the relatively low sample size used primarily for developing a method with rapid field data acquisition (i.e., photo-interpretation), fragmentation analysis provided valuable insights by revealing consistent trends in shape simplification. Our measurements were conducted within a river reach characterized by large alluvial bars and an active bank erosion process. It is important to note that

fragmentation rhythm and processes may differ significantly in headwater reaches where geomorphic and hydrological conditions vary. Additionally, the species of wood may influence the fragmentation process. Based on our observations, the samples primarily consisted of black poplar trees (*Populus nigra*), which are the most prevalent species in the study area. Standing trees were selected from vegetation patches that exhibit a representative height for our study area. This assumption is based on our experiences from monitoring activities conducted within the given river reach and even broader areas. The selected standing trees were closely located, with a reach spanning less than 5 km.

Practitioners often face decisions regarding wood removal without sufficient knowledge of wood transport conditions such as potential travel distance and the hydrological factors that trigger it. One significant factor influencing wood mobility is its size. Understanding the rate at which large woody elements fragment into smaller, more mobile pieces is crucial for informing decision-making. While the presence of large, geometrically complex wood pieces in rivers may not necessarily pose an issue, they can potentially block infrastructures such as bridges or dams. Knowledge of the speed of wood shape simplification could help predict the likelihood of a wood piece causing obstructions, as the risk increases with more intricately shaped elements. This is also true for the formation of jams. Conversely, if the objective is to enhance ecological benefits, the advantages associated with wood presence may diminish over time as its shape simplification progresses.

4.3 | Wood fragmentation and (im-)mobility

Whether or not a piece of wood is transported, can potentially affect the rate of morphological change. Merten et al. (2013) noted a higher incidence of breakage with greater travel distance. Our data does not permit statistical confirmation or refutation of this finding, but it does show that marked losses in branching complexity and related volume can occur even when travel distance is minimal or non-existent. We suggest that the quick change in form caused by fragmentation was the outcome of a collision with another transported log, as it was the highest part of the tree (i.e., furthest from the ground) that was dislodged. Chemical processes condition decomposition (Aristi et al., 2012; Iroumé, Ruiz-Villanueva, & Picco, 2017) accelerating physical changes over time, as do wetting and drying process, and temperature variations (Bilby et al., 1999; Wohl, 2013). As wood ages, sudden volume loss without mobility is likely to occur more frequently. Breakage of immobile wood became increasingly visible during the field campaigns, facilitating entrainment.

It is worth noting that one of the standing trees (074A8F) was transported into a jam, resulting in a drastic reduction of its branching complexity to 1. This observation suggests that the depositional context after the transport phase may also play a crucial role in shape simplification through dragging/rolling along the river bed. According to Harmon et al. (1986), the most decayed wood pieces are rarely found in jams. On the other hand, certain non-quantitative field observations indicate that simple shaped wood can be organised in jams. The question is whether the simplification of geometry is related to processes occurring prior to arrival in the jam (e.g., during transport) or to the accumulation process. The stability of the jam, especially when accumulated at bridge piers, may depend on the complexity of the shapes that constitute it. Additionally, branches aid in improving the cohesion of jam, ultimately reducing the likelihood of jam break-up (Lyn et al., 2003). Another potential parameter that could influence the susceptibility of a wood piece to breakage or debranching is its orientation to the flow. However, our data does not allow us to confirm this hypothesis. We observed that each of the wood pieces deposited isolated on alluvial bars was approximately parallel to the flow, whereas pieces that ended up in jams exhibited different orientations.

5 | CONCLUSION

In this paper we have considered methodological issues in assessing wood fragmentation in rivers using two different approaches. We have outlined their advantages and disadvantages, but both are seen as valuable and complementary. Our findings indicate that the debranching process is the primary driver of complexity change, which is very rapid during the first 2 years after injection into the river channel and then, it becomes negligible. Although the sample size was limited, our findings indicate that shape simplification can occur whether wood is transported or remains *in situ*. These observations possess significance for various river management practices, particularly the removal of large wood from watercourses. Nevertheless, to fully comprehend the mechanisms behind morphological adjustments due to fragmentation, we must obtain supplementary data from prolonged surveys in combination with studies of wood mobility. Future studies should integrate both field and laboratory investigations to comprehensively examine the physical breakdown processes during transport, as well as chemical, biological and weathering processes. Flume experiments could provide valuable insights into the precise mechanisms leading to branch fragility during desiccation, including the dominant hydraulic factors involved (e.g., velocity versus repeated branch movement against the flow).

AUTHOR CONTRIBUTIONS

Borbála Hortobágyi: a, c, d, h, i.
David Milan: a, b, c, d, i.
Fanny Bourgeau: a, c, d, h, i.
Hervé Piégay: a, b, c, d, g, i.

ACKNOWLEDGEMENTS

Borbála Hortobágyi received financial support from the French Biodiversity Agency (*Office Français de la Biodiversité*) and she acknowledges the financial and technical assistance provided by Véodis-3D consulting agency. We are grateful to the Val d'Allier National Natural Reserve (*Réserve Naturelle Nationale du Val d'Allier*) for their significant support. This study was conducted within the framework of EUR H_2O'Lyon (ANR-17-789 EURE-0018) at Université de Lyon, as part of the '*Investissements d'Avenir*' program operated by the French National Research Agency (ANR). David Milan conducted this research as an Institute of Advanced Studies Fellow funded through a Collegium de Lyon Fellowship, supported through H_2O'Lyon, Environment Ville Société, Fondation Réseau Français des Instituts d'Études Avancées, Grande Lyon la Métropole, Office Français de la Biodiversité, and the University of Hull. We express our

gratitude to the associate editor and the anonymous reviewers for their valuable comments, which have greatly contributed to the improvement of the manuscript.

DATA AVAILABILITY STATEMENT

The data that support the findings of this study are available from the corresponding author, BH, upon reasonable request.

ORCID

Borbála Hortobágyi https://orcid.org/0000-0002-0105-9456
David Milan https://orcid.org/0000-0002-9914-2134
Hervé Piégay https://orcid.org/0000-0002-3864-2119

REFERENCES

Abbe, T.B. & Montgomery, D.R. (1996) Large Woody debris jams, channel hydraulics and habitat formation in large Rivers. *Regulated Rivers: Research & Management*, 12(2-3), 201–221. Available from: https://doi.org/10.1002/(SICI)1099-1646(199603)12:2/3<201::AID-RRR390>3.0.CO;2-A

Abril, M., Muñoz, I., Casas-Ruiz, J.P., Gómez-Gener, L., Barceló, M., Oliva, F., et al. (2015) Effects of water flow regulation on ecosystem functioning in a Mediterranean river network assessed by wood decomposition. *Science of the Total Environment*, 517, 57–65. Available from: https://doi.org/10.1016/j.scitotenv.2015.02.015

Anlanger, C., Attermeyer, K., Hille, S., Kamjunke, N., Koll, K., König, M., et al. (2022) Large wood in river restoration: a case study on the effects on hydromorphology, biodiversity, and ecosystem functioning. *International Review of Hydrobiology*, 107(1-2), 34–45. Available from: https://doi.org/10.1002/iroh.202102089

Antonarakis, A.S., Richards, K.S., Brasington, J. & Bithell, M. (2009) Leafless roughness of complex tree morphology using terrestrial lidar. *Water Resources Research*, 45(10), 1–14. Available from: https://doi.org/10.1029/2008WR007666

Aristi, I., Díez, J.R., Larrañaga, A., Navarro-Ortega, A., Barceló, D. & Elosegi, A. (2012) Assessing the effects of multiple stressors on the functioning of Mediterranean rivers using poplar wood breakdown. *Science of the Total Environment, Integrated Modelling and Monitoring at Different River Basin Scales under Global Change*, 440, 272–279. Available from: https://doi.org/10.1016/j.scitotenv.2012.06.040

Beckman, N.D. & Wohl, E. (2014) Carbon storage in mountainous headwater streams: the role of old-growth forest and logjams. *Water Resources Research*, 50(3), 2376–2393. Available from: https://doi.org/10.1002/2013WR014167

Benke, A.C. & Wallace, J.B. (2003) Influence of wood on invertebrate communities in streams and rivers. In: Gregory, S.V., Boyer, K.L. & Gurnell, A.M. (Eds.) *The ecology and Management of Wood in world Rivers*. Maryland: Bethesda, pp. 149–177.

Bilby, R.E., Heffner, J.T., Fransen, B.R., Ward, J.W. & Bisson, P.A. (1999) Effects of immersion in water on deterioration of wood from five species of trees used for habitat enhancement projects. *North American Journal of Fisheries Management*, 19(3), 687–695. Available from: https://doi.org/10.1577/1548-8675(1999)019<0687:EOIIWO>2.0.CO;2

Bisson, P.A., Bilby, R.E., Bryant, M.D., Dolloff, C.A., Grette, G.B., House, R.A., et al. (1987) Large woody debris in forested streams in the Pacific Northwest: Past, present, and future. In: Salo, E.O. & Cundy, T.W. (Eds.) *Streamside management: forestry and fishery interactions*. Seattle, Washington: Institute of Forest Resources, University of Washington, pp. 143–190.

Boivin, M., & Buffin-Bélanger, T. (2010) Using a terrestrial LiDAR for monitoring of large woody debris jams in gravel-bed rivers.

Braccia, A. & Batzer, D.P. (2008) Breakdown and invertebrate colonization of dead wood in wetland, upland, and river habitats. *Canadian Journal of Forest Research*, 38(10), 2697–2704. Available from: https://doi.org/10.1139/X08-113

Brodu, N. & Lague, D. (2012) 3D terrestrial lidar data classification of complex natural scenes using a multi-scale dimensionality criterion: applications in geomorphology. *ISPRS Journal of Photogrammetry and Remote Sensing*, 68, 121–134. Available from: https://doi.org/10.1016/j.isprsjprs.2012.01.006

Cadol, D. & Wohl, E. (2010) Wood retention and transport in tropical, headwater streams, La Selva Biological Station, Costa Rica. *Geomorphology*, 123(1-2), 61–73. Available from: https://doi.org/10.1016/j.geomorph.2010.06.015

Collier, K.J. (2014) Wood decay rates and macroinvertebrate community structure along contrasting human pressure gradients (Waikato, New Zealand). *New Zealand Journal of Marine and Freshwater Research*, 48(1), 97–111. Available from: https://doi.org/10.1080/00288330.2013.847470

Comiti, F., Andreoli, A., Lenzi, M.A. & Mao, L. (2006) Spatial density and characteristics of woody debris in five mountain rivers of the Dolomites (Italian Alps). *Geomorphology*, 78(1-2), 44–63. Available from: https://doi.org/10.1016/j.geomorph.2006.01.021

Conley, W. & Kramer, N. (2020) Riverine large wood and recreation safety: a framework to discretize and contextualize hazard. *Earth Surface Processes and Landforms*, 45(9), 2201–2216. Available from: https://doi.org/10.1002/esp.4862

De Cicco, P.N., Paris, E., Ruiz-Villanueva, V., Solari, L. & Stoffel, M. (2018) In-channel wood-related hazards at bridges: a review. *River Research and Applications*, 34(7), 617–628. Available from: https://doi.org/10.1002/rra.3300

Demol, M., Wilkes, P., Raumonen, P., Krishna Moorthy, S.M., Calders, K., Gielen, B., et al. (2022) Volumetric overestimation of small branches in 3D reconstructions of *Fraxinus excelsior*. *Silva Fennica*, 56(1), 10550. Available from: https://doi.org/10.14214/sf.10550

Díez, J., Elosegi, A., Chauvet, E. & Pozo, J. (2002) Breakdown of wood in the Agüera stream. *Freshwater Biology*, 47(11), 2205–2215. Available from: https://doi.org/10.1046/j.1365-2427.2002.00965.x

Fan, G., Nan, L., Dong, Y., Su, X. & Chen, F. (2020) AdQSM: a new method for estimating above-ground biomass from TLS point clouds. *Remote Sensing*, 12(18), 3089. Available from: https://doi.org/10.3390/rs12183089

Gonzalez de Tanago, J., Lau, A., Bartholomeus, H., Herold, M., Avitabile, V., Raumonen, P., et al. (2018) Estimation of above-ground biomass of large tropical trees with terrestrial LiDAR. *Methods in Ecology and Evolution*, 9(2), 223–234. Available from: https://doi.org/10.1111/2041-210X.12904

Grabowski, R.C., Gurnell, A.M., Burgess-Gamble, L., England, J., Holland, D., Klaar, M.J., et al. (2019) The current state of the use of large wood in river restoration and management. *Water and Environment Journal Wej.12465*, 33(3), 366–377. Available from: https://doi.org/10.1111/wej.12465

Grigillo, D., Vrečko, A., Mikoš, M., Gvozdanović, T., Anžur, A., Vezočnik, R., et al. (2015) Determination of Large Wood Accumulation in a Steep Forested Torrent Using Laser Scanning. In: Lollino, G., Arattano, M., Rinaldi, M., Giustolisi, O., Marechal, J.-C. & Grant, G.E. (Eds.) *Engineering geology for society and territory - volume 3*. Cham: Springer International Publishing, pp. 127–130. https://doi.org/10.1007/978-3-319-09054-2_24

Gurnell, A., England, J. & Burgess-Gamble, L. (2019) Trees and wood: working with natural river processes. *Water and Environment Journal*, 33(3), 342–352. Available from: https://doi.org/10.1111/wej.12426

Gurnell, A.M., Piégay, H., Swanson, F.J. & Gregory, S.V. (2002) Large wood and fluvial processes. *Freshwater Biology*, 47(4), 601–619. Available from: https://doi.org/10.1046/j.1365-2427.2002.00916.x

Hackenberg, J. (2019) *The simple Forest handbook. A user guide for QSM building*. Hoboken, NJ, USA: Wiley.

Hackenberg, J., Disney, M., Bontemps, J.-D. (2022) Gaining insight into the allometric scaling of trees by utilizing 3d reconstructed tree models - a SimpleForest study. https://doi.org/10.1101/2022.05.05.490069

Hackenberg, J., Morhart, C., Sheppard, J., Spiecker, H. & Disney, M. (2014) Highly accurate tree models derived from terrestrial laser scan data: a method description. *Forests*, 5(5), 1069–1105. Available from: https://doi.org/10.3390/f5051069

Hackenberg, J., Spiecker, H., Calders, K., Disney, M. & Raumonen, P. (2015) SimpleTree —an efficient open source tool to build tree models from TLS clouds. *Forests*, 6(12), 4245–4294. Available from: https://doi.org/10.3390/f6114245

Hackenberg, J., Wassenberg, M., Spiecker, H. & Sun, D. (2015) Non destructive method for biomass prediction combining TLS derived tree volume and wood density. *Forests*, 6(12), 1274–1300. Available from: https://doi.org/10.3390/f6041274

Harmon, M.E., Franklin, J.F., Swanson, F.J., Sollins, P., Gregory, S.V., Lattin, J.D., et al. (1986) Ecology of coarse Woody debris in temperate ecosystems. *Advances in Ecological Research*, 15, 133–302. Available from: https://doi.org/10.1016/S0065-2504(08)60121-X

Horton, R.E. (1932) Drainage-basin characteristics. *Eos, Transactions American Geophysical Union*, 13(1), 350–361. Available from: https://doi.org/10.1029/TR013i001p00350

Iroumé, A., Ruiz-Villanueva, V. & Picco, L. (2017) Breakdown of instream wood in low order forested streams of the southern Chilean mountain ranges. *Forest Ecology and Management*, 401, 17–32. Available from: https://doi.org/10.1016/j.foreco.2017.06.058

Järvelä, J. (2004) Determination of flow resistance caused by non-submerged woody vegetation. *International Journal of River Basin Management*, 2(1), 61–70. Available from: https://doi.org/10.1080/15715124.2004.9635222

Kaiser, A., Neugirg, F., Rock, G., Müller, C., Haas, F., Ries, J., et al. (2014) Small-scale surface reconstruction and volume calculation of soil erosion in complex Moroccan gully morphology using structure from motion. *Remote Sensing*, 6(8), 7050–7080. Available from: https://doi.org/10.3390/rs6087050

Kramer, N. & Wohl, E. (2017) Rules of the road: a qualitative and quantitative synthesis of large wood transport through drainage networks. *Geomorphology*, 279, 74–97. Available from: https://doi.org/10.1016/j.geomorph.2016.08.026

Lyn, D.A., Cooper, T., Yi, Y.-K., Sinha, R., & Rao, A.R. (2003) Debris accumulation at bridge crossings, laboratory and field studies (No. FHWA/IN/JTRP-2003/10).

Mancini, F., Dubbini, M., Gattelli, M., Stecchi, F., Fabbri, S. & Gabbianelli, G. (2013) Using unmanned aerial vehicles (UAV) for high-resolution reconstruction of topography: the structure from motion approach on coastal environments. *Remote Sensing*, 5(12), 6880–6898. Available from: https://doi.org/10.3390/rs5126880

Manners, R.B., Doyle, M.W. & Small, M.J. (2007) Structure and hydraulics of natural woody debris jams. *Water Resources Research*, 43(6), 1–17. Available from: https://doi.org/10.1029/2006WR004910

Merten, E.C., Vaz, P.G., Decker-Fritz, J.A., Finlay, J.C. & Stefan, H.G. (2013) Relative importance of breakage and decay as processes depleting large wood from streams. *Geomorphology*, 190, 40–47. Available from: https://doi.org/10.1016/j.geomorph.2013.02.006

Montgomery, D.R., Collins, B.D., Buffington, J.M. & Abbe, T.B. (2003) Geomorphic effects of wood in Rivers. *American Fisheries Society Symposium*, 2003, 21–47.

Newbrey, M.G., Bozek, M.A., Jennings, M.J. & Cook, J.E. (2005) Branching complexity and morphological characteristics of coarse woody structure as lacustrine fish habitat. *Canadian Journal of Fisheries and Aquatic Sciences*, 62(9), 2110–2123. Available from: https://doi.org/10.1139/f05-125

Piégay, H. & Gurnell, A.M. (1997) Large woody debris and river geomorphological pattern: examples from S.E. France and S. England. *Geomorphology*, 19(1-2), 99–116. Available from: https://doi.org/10.1016/S0169-555X(96)00045-1

Piégay, H. & Landon, N. (1997) Promoting ecological management of riparian forests on the Drôme River, France. *Aquatic Conservation: Marine and Freshwater Ecosystems*, 7(4), 287–304. Available from: https://doi.org/10.1002/(SICI)1099-0755(199712)7:4<287::AID-AQC247>3.0.CO;2-S

R Core Team. (2022) A language and environment for statistical computing.

Ravazzolo, D., Spreitzer, G., Tunnicliffe, J. & Friedrich, H. (2022) The effect of large wood accumulations with Rootwads on local geomorphic changes. *Water Resources Research*, 58(5), e2021WR031403. Available from: https://doi.org/10.1029/2021WR031403

Ruiz-Villanueva, V., Aarnink, J., Ghaffarian, H., Gibaja del Hoyo, J., Finch, B., Hortobágyi, B., et al. (2024) Current progress in quantifying and monitoring instream large wood supply and transfer in rivers. *Earth Surface Processes and Landforms*, 49(1), 256–276. Available from: https://doi.org/10.1002/esp.5765

Ružić, I., Marović, I., Benac, Č. & Ilić, S. (2014) Coastal cliff geometry derived from structure-from-motion photogrammetry at Stara Baška, Krk Island, Croatia. *Geo-Marine Letters*, 34(6), 555–565. Available from: https://doi.org/10.1007/s00367-014-0380-4

Sanhueza, D., Picco, L., Paredes, A. & Iroumé, A. (2022) A faster approach to quantify large wood using UAVs. *Drones*, 6(8), 218. Available from: https://doi.org/10.3390/drones6080218

Schalko, I. (2017) Large wood accumulation probability at a single bridge pier. In: *Proceedings of the 37th IAHR World Congress. Presented at the 37th IAHR World Congress: Learning from the Past for the Future, ETH Zurich, Kuala Lumpur, Malaysia*, pp. 1704–1713. Available from: https://doi.org/10.3929/ETHZ-B-000185312

Schwendel, A.C. & Milan, D.J. (2020) Terrestrial structure-from-motion: spatial error analysis of roughness and morphology. *Geomorphology*, 350, 106883. Available from: https://doi.org/10.1016/j.geomorph.2019.106883

Sear, D.A., Millington, C.E., Kitts, D.R. & Jeffries, R. (2010) Logjam controls on channel:floodplain interactions in wooded catchments and their role in the formation of multi-channel patterns. *Geomorphology, Geomorphology and Vegetation: Interactions, Dependencies, and Feedback Loops*, 116(3-4), 305–319. Available from: https://doi.org/10.1016/j.geomorph.2009.11.022

Senter, A.E. & Pasternack, G.B. (2011) Large wood aids spawning Chinook salmon (Oncorhynchus tshawytscha) in marginal habitat on a regulated river in California. *River Research and Applications*, 27(5), 550–565. Available from: https://doi.org/10.1002/rra.1388

Spreitzer, G., Tunnicliffe, J. & Friedrich, H. (2019) Using structure from motion photogrammetry to assess large wood (LW) accumulations in the field. *Geomorphology*, 346, 106851. Available from: https://doi.org/10.1016/j.geomorph.2019.106851

Spreitzer, G., Tunnicliffe, J. & Friedrich, H. (2020) Large wood (LW) 3D accumulation mapping and assessment using structure from motion photogrammetry in the laboratory. *Journal of Hydrology*, 581, 124430. Available from: https://doi.org/10.1016/j.jhydrol.2019.124430

Spreitzer, G., Tunnicliffe, J. & Friedrich, H. (2020) Porosity and volume assessments of large wood (LW) accumulations. *Geomorphology*, 358, 107122. Available from: https://doi.org/10.1016/j.geomorph.2020.107122

Stovall, A.E.L., Anderson-Teixeira, K.J. & Shugart, H.H. (2018) Assessing terrestrial laser scanning for developing non-destructive biomass allometry. *Forest Ecology and Management*, 427, 217–229. Available from: https://doi.org/10.1016/j.foreco.2018.06.004

Strahler, A.N. (1957) Quantitative analysis of watershed geomorphology. *Eos, Transactions American Geophysical Union*, 38(6), 913–920. Available from: https://doi.org/10.1029/TR038i006p00913

Tonon, A., Picco, L., Ravazzolo, D. & Lenzi, M.A. (2014) Using a terrestrial laser scanner to detect wood characteristics in gravel-bed rivers. *Journal of Agricultural Engineering*, 45(4), 161–167. Available from: https://doi.org/10.4081/jae.2014.431

Welber, M., Bertoldi, W. & Tubino, M. (2013) Wood dispersal in braided streams: results from physical modeling. *Water Resources Research*, 49(11), 7388–7400. Available from: https://doi.org/10.1002/2013WR014046

Wohl, E. (2013) Floodplains and wood. *Earth-Science Reviews*, 123, 194–212. Available from: https://doi.org/10.1016/j.earscirev.2013.04.009

Wohl, E., Hall, R.O., Lininger, K.B., Sutfin, N.A. & Walters, D.M. (2017) Carbon dynamics of river corridors and the effects of human alterations. *Ecological Monographs*, 87(3), 379–409. Available from: https://doi.org/10.1002/ecm.1261

Wohl, E., Kramer, N., Ruiz-Villanueva, V., Scott, D.N., Comiti, F., Gurnell, A.M., et al. (2019) The natural wood regime in Rivers. *Bioscience*, 69(4), 259–273. Available from: https://doi.org/10.1093/biosci/biz013

Wohl, E., Uno, H., Dunn, S.B., Kemper, J.T., Marshall, A., Means-Brous, M., et al. (2023) Why wood should move in rivers. *River Research and Applications*, 4114. Available from: https://doi.org/10.1002/rra.4114

How to cite this article: Hortobágyi, B., Milan, D., Bourgeau, F. & Piégay, H. (2024) How quickly does wood fragment in rivers? Methodological challenges, preliminary findings, and perspectives. *Earth Surface Processes and Landforms*, 1–20. Available from: https://doi.org/10.1002/esp.5877